ISSN: 2414-1895 DOI: 10.6919/ICJE.202506_11(6).0044

Revealing the Electrical Characteristic Distribution of Internal Functional Layers in InGaAs/InP Avalanche Photodiodes

Yue Cheng[1], Feiyu Mao[2], Jiayu Meng[3]

[1] School of Materials and Chemistry, University of Shanghai for Science and Technology, Shanghai, 200093, China

[2] School of Microelectronics, Shanghai University, Shanghai 201899, China

[3] School of Science, University of Shanghai for Science and Technology, Shanghai, 200093, China

Abstract

This study systematically analyzed the electrical characteristic distribution of internal functional layers in InGaAs/InP avalanche photodiodes (APDs) and their correlation with Zn diffusion processes using cross-sectional scanning probe microscopy (SPM). Experimental results revealed a 536 mV surface potential difference at the InGaAs absorption layer/InP cap layer interface, primarily attributed to differences in electron affinitand bandgap, with Zn diffusion inducing a transition in carrier response from electron-dominated to hole-dominated behavior. The 7.3 μm lateral diffusion width exceeded the design specification due to lattice dynamics, while the 1.6 μm longitudinal diffusion depth demonstrated precise control, effectively optimizing electric field uniformity and suppressing edge breakdown. Furthermore, the unintentionally doped InGaAs absorption layer exhibited pronounced sensitivity to photoexcitation, unveiling a mechanism for light-regulated enhancement of minority carrier dynamics. By establishing a quantitative link between nanoscale electrical properties and Zn diffusion kinetics, this work provides critical insights for optimizing fabrication processes and reliability designs of high-performance APDs, advancing their applications in optical communications and quantum detection systems.

Keywords

InGaAs/InP APD; SPM; Zn Diffusion; Carrier Distribution; Surface Potential Distribution.

1. Introduction

Avalanche photodiodes (APDs), as core devices for optical signal detection, play an irreplaceable role in fields such as optical communications, lidar, and quantum sensing [1–4]. Among these, InGaAs/InP APDs have emerged as the preferred solution for high-speed, high-sensitivity photodetection due to their wide spectral response, high gain characteristics, and low dark current. However, as performance requirements for these devices escalate in advanced applications, the design of their multilayer heterostructures and the precise control of doping processes face significant challenges. Specifically, the Zn diffusion process critically governs the internal electric field distribution, carrier transport, and band structure modulation at interfaces, which directly determine the breakdown characteristics, gain uniformity, and long-term reliability of APDs[5–7].

Conventional electrical characterization techniques, such as capacitance-voltage (C-V) profiling and secondary ion mass spectrometry (SIMS), provide macroscopic doping concentration information but fail to resolve localized carrier behavior at heterointerfaces, surface state distributions, or microscale

ISSN: 2414-1895 DOI: 10.6919/ICJE.202506_11(6).0044

potential fluctuations induced by diffusion processes[8–11]. Additionally, destructive sample preparation methods may introduce defect, leading to deviations between analytical results and the true operational state of devices. In recent years, advances in scanning probe microscopy (SPM) have enabled novel pathways for nanoscale electrical characterization[12–14]: scanning capacitance microscopy (SCM) maps carrier type and concentration distributions in real time by detecting differential capacitance signals[15–17], while Kelvin probe force microscopy (KPFM) non-invasively measures surface potentials and band alignments[18–20]. The combined application of these techniques allows for *in situ*, high-resolution characterization of cross-sectional electrical properties in devices. However, the complex multilayer heterostructure of InGaAs/InP APDs and the impact of Zn diffusion processes on interfacial carrier dynamics and electric field distributions remain insufficiently resolved, hindering a comprehensive understanding of performance-limiting mechanisms.

This study focuses on separated absorption, grading, charge, and multiplication (SAGCM) type InGaAs/InP APDs, employing a cross-sectional SPM strategy integrated with SCM and KPFM. Through in situ nanoscale-resolution characterization, we systematically resolve the carrier distribution, interfacial potential, and Zn diffusion doping behavior within the device. The work aims to elucidate the regulatory mechanisms of Zn diffusion processes on electrical properties, particularly their impact on electric field uniformity and carrier transport dynamics. These insights establish a nanoscale structure-property correlation, providing a theoretical foundation for optimized APD design and reliability enhancement in high-sensitivity applications such as optical communications and quantum sensing.

2. Experiments

2.1 Sample Preparation

The SAGCM-type InGaAs/InP APDs in this study were epitaxially grown on an n^+-InP substrate using metal-organic chemical vapor deposition (MOCVD). The epitaxial layer structure, as illustrated in Figure 1, sequentially comprises the following layers along the growth direction: an n^+-InP substrate, an n^--InP buffer layer, an i-InGaAs absorption layer, an i-InGaAsP grading layer, an n^--InP charge layer, and an i-InP cap layer. Zn diffusion within the cap layer formed a dual p-type diffusion zone and a floating guard ring (FGR) structure, further dividing the cap layer into an i-InP multiplication layer and a p^+-InP Zn-diffused layer.

For cross-sectional characterization, samples were prepared by cleaving the InGaAs/InP APD devices along the crystal orientation using a thin surgical blade. Controlled mechanical pressure was applied to the backside to induce natural fracture, ensuring that the resulting cross-section achieved nanometer-scale flatness while traversing the center of the active region on the sample surface. The cleaved samples were then mounted onto steel substrates using conductive silver epoxy, with the cleaved surface aligned parallel to the horizontal plane. After curing, the samples were placed onto the characterization platform for subsequent analysis.

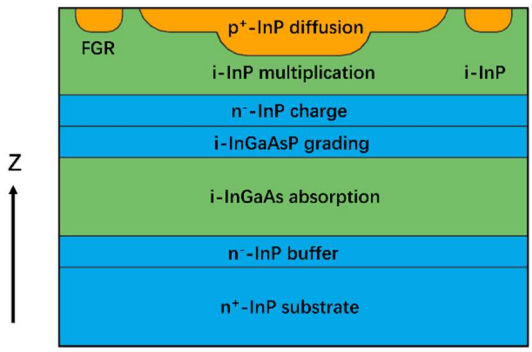

Figure 1. Schematic diagram of the InGaAs/InP APD structure along the growth direction (Z)

ISSN: 2414-1895 DOI: 10.6919/ICJE.202506_11(6).0044

2.2 SPM Characterization

In this study, the test samples were characterized using cross-sectional SPM techniques, including both SCM and KPFM. Based on their distinct measurement principles, KPFM required immediate testing of prepared samples in a nitrogen-purged environment to prevent surface contamination, while SCM necessitated exposing the cleaved surface of InGaAs/InP APD to ambient air for approximately 30 minutes to form a natural oxide adsorption layer as an insulating layer prior to characterization. For KPFM measurements, a heavily doped silicon probe (RTESP-300) with a tip radius of 8 nm was employed, featuring a cantilever resonant frequency of 300 kHz and a spring constant of 40 N/m. SCM measurements utilized a diamond-coated Si probe (CDT-NCLR) with a spring constant of ~72 N/m, where a 1 V AC bias at 90 kHz was applied during testing while maintaining a fixed DC bias of 0 V..

3. Results and Discussion

3.1 SPM Characterization of the Cross-sectional InGaAs/InP Materials

Figure 2 presents cross-sectional SPM characterization of the InGaAs/InP material region prior to Zn diffusion, where SCM and KPFM were primarily employed to analyze carrier behavior, potential distribution, and the influence of potential defects or interface states at the interface. Figures 2(b) and 2(c) show SCM and KPFM images of the InGaAs/InP material, respectively, enabling clear distinction between the intrinsically doped InGaAs absorption layer and the InP cap layer.

In SCM characterization, a positive dC/dV signal indicates a hole-dominated response in the measured region, while a negative signal corresponds to an electron-dominated response. The amplitude of the dC/dV signal inversely correlates with local carrier concentration, providing intuitive insights into carrier density. As shown in Figure 2(d), the dC/dV profile across the functional layers of the InGaAs/InP APD exhibits uniformly negative signals, suggesting electron-dominated responses throughout the structure.

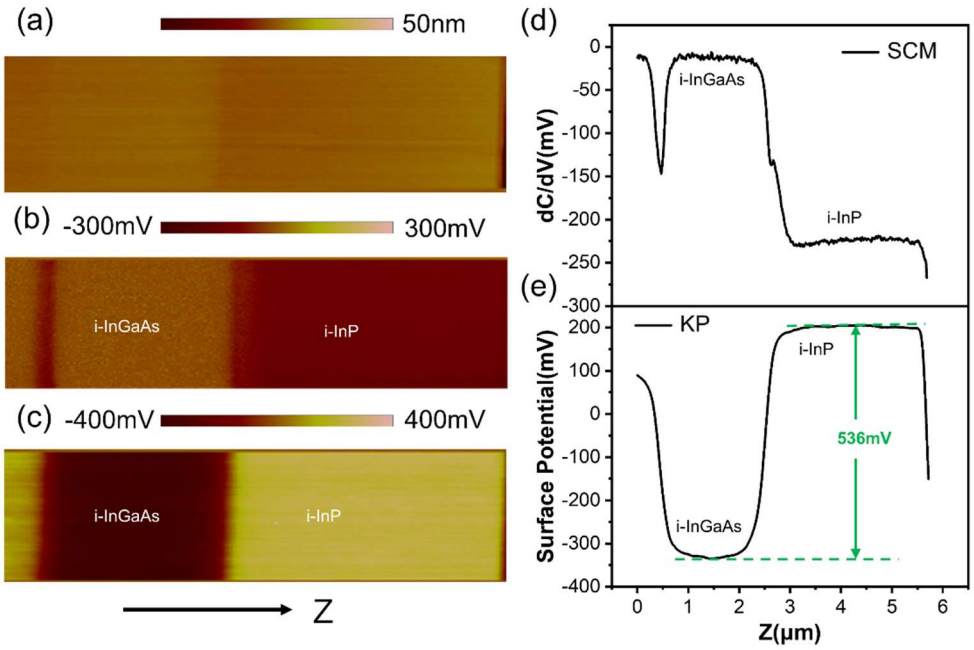

Figure 2. SPM characterization of InGaAs/InP materials. (a) AFM image; (b) SCM image; (c) KPFM image; (d) dC/dV distribution curve along the growth direction; (e) surface potential distribution curve along the growth direction

ISSN: 2414-1895 DOI: 10.6919/ICJE.202506_11(6).0044

Figure 2(e) reveals a surface potential difference of approximately 536 mV at the InGaAs/InP interface, attributed to their intrinsic material properties. The InP cap layer exhibits higher surface potential due to its greater electron affinity (4.4 eV) compared to InGaAs (4.0 eV). The wide bandgap of InP (1.35 eV) positions its Fermi level closer to the conduction band (n-type characteristics), while the narrow bandgap of InGaAs (0.75 eV) shifts its Fermi level toward the valence band (p-type characteristics), resulting in significant band offset at the interface. Additionally, the lower surface state density of InP minimizes Fermi-level pinning, allowing its surface potential to approach intrinsic values. In contrast, InGaAs may experience partial Fermi-level pinning due to surface charge accumulation or oxide layer effects.

3.2 SPM Characterization of the Cross-sectional InGaAs/InP APD

Precise control of Zn diffusion is critical for achieving high-performance APDs, directly influencing their application efficacy in optical communications, LiDAR, and quantum detection. This study focuses on SPM characterization of Zn diffusion at the floating guard ring (FGR) region of InGaAs/InP APDs. The FGR, encircling the device periphery, homogenizes electric field distribution, suppresses edge breakdown, and enhances breakdown voltage and reliability. Figure 3(a) displays an AFM image of the cleaved InGaAs/InP APD surface, demonstrating relatively flat topography. The corresponding SCM image in Figure 3(b) reveals a well-defined FGR profile formed by Zn diffusion. While the designed diffusion window during fabrication was 5 μm, Figure 3(c) shows the maximum diffusion width reaching 7.3 μm. This discrepancy arises because Zn diffusion follows a slow, concentration-gradient-dependent solid-state diffusion process, governed collectively by material lattice dynamics, thermal gradients, and microscopic edge morphology of the diffusion mask. In InP crystals, Zn migration relies on a vacancy-assisted mechanism, where alternating movement between lattice interstitials and substitutional sites induces asymmetric broadening at the diffusion front. Such lateral expansion becomes pronounced during prolonged high-temperature processing, ultimately causing the actual diffusion window to exceed its designed dimensions.

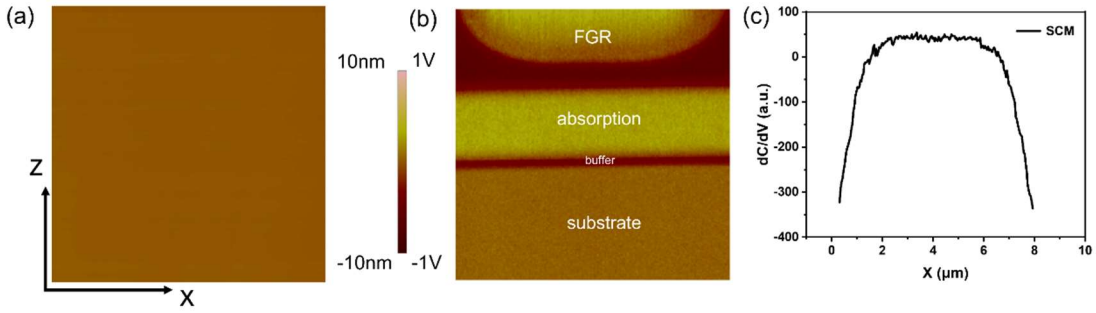

Figure 3. SPM characterization of the cross-sectional InGaAs/InP APD. (a) AFM image; (b) SCM image; (c) FGR-derived dC/dV curve along the X-direction.

Figure 4 highlights the significance of Zn diffusion depth (Z-direction) compared to lateral diffusion studies in the FGR region, with the most notable distinction from Figure 2 being the Zn-diffused region. In Figure 4(d), the dC/dV profile reveals a hole-dominated response in the InGaAs/InP material due to Zn diffusion. Similarly, KPFM characterization demonstrates that Zn incorporation as an acceptor impurity in InP introduces acceptor levels within the bandgap, shifting the Fermi level toward the valence band and thereby reducing the surface potential in the doped region. Figures 4(d) and 4(e) illustrate carrier distribution and surface potential profiles across the functional layers of the InGaAs/InP APD. Auxiliary guidelines in Figure 4 confirm strong consistency between SCM and KPFM results in delineating the device's functional regions. Both samples exhibit a 200 nm buffer layer, a 2 μm absorption layer, and a Zn diffusion depth of approximately 1.6 μm at the InGaAs/InP floating guard ring, closely aligning with the initial design specifications.

ISSN: 2414-1895 DOI: 10.6919/ICJE.202506_11(6).0044

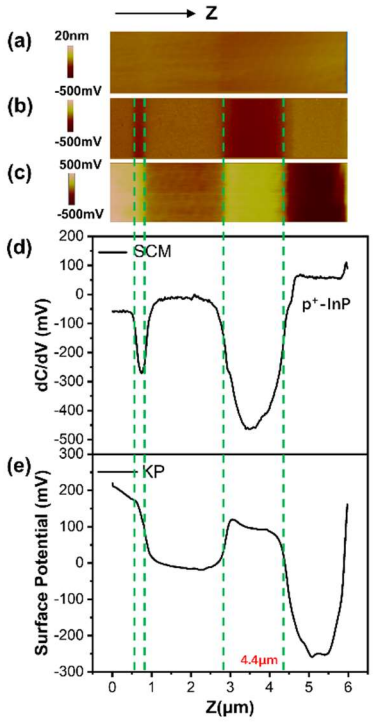

Figure 4. SPM characterization of functional layers in InGaAs/InP APD. (a) AFM image; (b) SCM image; (c) KPFM image; (d) dC/dV distribution curve along the growth direction; (e) surface potential distribution curve along the growth direction

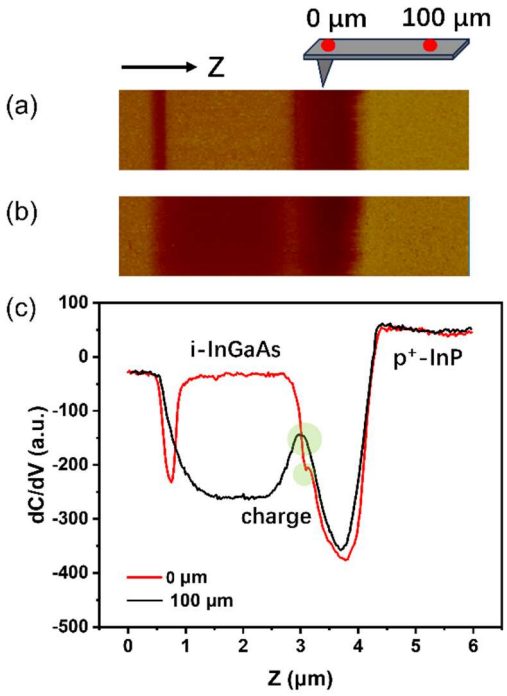

Figure 5. (a) SCM image with AFM spot at 0 μm probe cantilever position; (c) SCM image with AFM spot at 100 μm probe position; (e) dC/dV curves along the growth direction under varying AFM spot positions

In SCM measurements, the AFM system's laser spot is conventionally positioned at the 0 μm location on the probe cantilever to sensitively detect tip-sample contact forces. Here, the cantilever position at 100 μm was compared with the standard spot location, as illustrated in Figure 5. Notably, the

ISSN: 2414-1895 DOI: 10.6919/ICJE.202506_11(6).0044

maximum variation in dC/dV signals between the two spot positions (0 μm vs. 100 μm) occurs in the unintentionally doped InGaAs absorption layer, while negligible signal differences are observed in other doped regions. At the 100 μm spot position, the differential capacitance signal in the i-InGaAs absorption layer reflects its weakly intrinsic characteristics, accentuating the charge layer due to its relatively higher n-type doping (light green region, Figure 5(c)). This feature is also detectable at the 0 μm spot position, just less pronounced. The observed dC/dV profile shifts between 0 μm and 100 μm spot positions indicate heightened sensitivity of the absorption layer to laser illumination. The photoexcitation conditions enhance the response cycle of minority carriers, enabling their effective interaction with the rapidly alternating AC bias.

4. Conclusion

This study systematically reveals the electrical characteristic distributions of functional layers in SAGCM-type InGaAs/InP APDs and their correlations with Zn diffusion processes through cross-sectional SPM characterization techniques, with main conclusions as follows:

(1) A 536 mV potential difference emerges at the InGaAs/InP interface due to intrinsic material differences, while SCM confirms the carrier type transition from electron-dominated to hole-dominated response after Zn diffusion.

(2) The asymmetric broadening manifested by 7.3 μm lateral diffusion unveils the coupling effects between lattice dynamics and process parameters, whereas the precisely controlled 1.6 μm longitudinal depth demonstrates process-designable vertical electric fields. Their synergistic optimization enhances device edge breakdown resistance.

(3) The unintentionally doped InGaAs absorption layer exhibits high sensitivity to photoexcitation, providing new perspectives for photo-controlled carrier transport and low-noise detection.

This research not only establishes an innovative methodology for microscopic electrical analysis of APDs, but also proposes explicit optimization pathways through process-structure-performance correlations, offering direct guidance for developing high-reliability optoelectronic devices.

References

[1] H. Wang, Y. Gu, C. Yu, et al. Direct correlation of defects and dark currents of InGaAs/InP photodetectors, Materials Science in Semiconductor Processing, vol. 123 (2021), 105540.

[2] P. Martyniuk, P. Wang, A. Rogalski, Y. Gu, et al. W. Hu, Infrared avalanche photodiodes from bulk to 2D materials, Light Sci Appl, vol. 12 (2023), 212.

[3] J. Zang, J.S. Morgan, X. Xie, K. Sun, et al. InP/InGaAs Photovaractor, Journal of Lightwave Technology, vol. 36 (2018), 1661–1665.

[4] O.M. Braga, C.A. Delfino, R.M.S. Kawabata, et al. Investigation of InGaAs/InP photodiode surface passivation using epitaxial regrowth of InP via photoluminescence and photocurrent, Materials Science in Semiconductor Processing, vol. 154 (2023), 107200.

[5] I. Yun, K.-S. Hyun. Zinc diffusion process investigation of InP-based test structures for high-speed avalanche photodiode fabrication, Microelectronics Journal 31 (2000) 635–639.

[6] N. Chand, P.A. Houston. Diffusion of Cd And Zn In InP between 550 and 650°C, J. Electron. Mater, vol. 11 (1982), 37–52.

[7] R. Jakiela, Phosphorus vacancy mediated complex diffusion mechanism of Zn in InP, Materials Letters, vol. 335 (2023), 133835.

[8] E.G. Seebauer, D.E. Barlaz. SIMS for analysis of nanostructures, Current Opinion in Chemical Engineering, vol. 12 (2016), 8–13.

[9] N.P. Lockyer, S. Aoyagi, J.S. Fletcher, et al. Secondary ion mass spectrometry, Nat Rev Methods Primers, vol. 4 (2024), 1–21.

[10] G. Sozzi, G. Chiorboli, L. Perini, et al. Investigating Mesa Structure Impact on C-V Measurements, IEEE Access, vol. 12 (2024), 32938–32943.

ISSN: 2414-1895 DOI: 10.6919/ICJE.202506_11(6).0044

[11] J. Zheng, Y. Zhou, Y. Zhang, et al. C-V characteristics of piezotronic metal-insulator-semiconductor transistor, Science Bulletin, vol. 65 (2020), 161–168.

[12] D. Marinskiy, P. Edelman, J. Lagowski, et al. Kelvin Force Microscopy and corona charging for semiconductor material and device characterization, Superlattices and Microstructures, vol. 99 (2016), 13–23.

[13] U. Celano, F.-C. Hsia, D. Vanhaeren, K. Paredis, et al. Mesoscopic physical removal of material using sliding nano-diamond contacts, Sci Rep, vol. 8 (2018), 2994.

[14] K. Bian, C. Gerber, A.J. Heinrich, et al.Scanning probe microscopy, Nat Rev Methods Primers, vol. 1 (2021), 1–29.

[15] R. Coq Germanicus, F. Lallemand, D. Chateigner, et al. Dopant activity for highly in-situ doped polycrystalline silicon: hall, XRD, scanning capacitance microscopy (SCM) and scanning spreading resistance microscopy (SSRM), Nano Ex, vol. 2 (2021), 010037.

[16] M.J. Kappers, T. Zhu, S.-L. Sahonta, et al. SCM and SIMS investigations of unintentional doping in III-nitrides, Physica Status Solidi C Current Topics, vol. 12 (2015), 403–407.

[17] V.V. Zavyalov, J.S. McMurray, C.C. Williams. Scanning capacitance microscope methodology for quantitative analysis of p-n junctions, Journal of Applied Physics, vol. 85 (1999), 7774–7783.

[18] Z. Qu, J. Wei, X. Liu, et al. Atomic structure and electron distribution of Co atoms adsorbed on Si(111) surface by NC-AFM/KPFM at 78 K, Surface Science, vol. 724 (2022), 122130.

[19] S. Sadewasser. Surface potential of chalcopyrite films measured by KPFM, Physica Status Solidi (a), vol. 203 (2006), 2571–2580.

[20] W. Melitz, J. Shen, A.C. Kummel, S. Lee. Kelvin probe force microscopy and its application, Surface Science Reports, vol. 66 (2011), 1–27.